Article

A Geometric-based Aerodynamic Roughness Length Formulation and Code Applied to Lidar-derived Snow Surfaces

Rachel A Neville , Patrick D Shipman , Steven R Fassnacht [*] , Jessica E. Sanow , Ron Pasquini , Iuliana Oprea

Article

A Geometric-based Aerodynamic Roughness Length Formulation and Code Applied to Lidar-Derived Snow Surfaces

Rachel Neville [1] , Patrick D. Shipman [2], Steven R. Fassnacht [3,4,*], Jessica E. Sanow [3], Ron Pasquini [5], and Iuliana Oprea [5]

[1]   Department of Mathematics and Statistics, Northern Arizona University
[2]   Department of Mathematics; GIDP in Applied Mathematics
[3]   ESS-Watershed Science, Colorado State University
[4]   ESS-Watershed Science, Colorado State University; Cooperative Institute for Research into the Atmosphere
[5]   Department of Mathematics, Colorado State University
[*]   Correspondence: steven.fassnacht@colostate.edu; Tel.: +001-970-491-5454

Abstract: The roughness of the Earth's surface dictates the nature of air flow across it. During some parts of the year, a large portion of the Earth's surface is snow covered, and the roughness of the snow surface varies over the snow season and over space. Detailed meteorological data that are necessary to access the aerodynamic roughness (z_0) are not widely collected and as such the geometry of a surface can be used to estimate z_0. Here we present a formulation and the corresponding computer code to compute z_0 based on the Lettau (1969) geometric approach. We apply it to three snow surface datasets, each at different phases of the snowpack (and each at two resolutions): fresh snow accumulation (1 m^2 at 1 and 10 mm), peak accumulation (1 km^2 at 1 and 10 m) and ablation sun cups (25 m^2 at 5 and 50 mm). The new code produces a mean z_0, as well as a histogram of all z_0 values for each individual roughness element (10s of thousand for the 1000 x 1000 grids), as well as directional z_0 diagrams, which can be matches with the wind rose for the location. The formulation includes two parameters that may optionally be applied to smooth the surface before calculating z_0. By calculating z_0 as a function of these two parameters, we demonstrate the sensitivity of the z_0 value to these parameter choices.

Keywords: z_0; Lettau geometry z_0; snow roughness

1. Introduction

      Shallow, seasonal snowpack is a critical reservoir for yearly water yield in the western US [1,2]. The snowpack acts as a temporary water storage system and is essential for all regional hydrology, influencing water availability for all natural ecosystems, agricultural, urban systems. Consequently, precise modeling of snowpack dynamics is crucial for accurate estimations of snowmelt [3]. Within hydrologic and cryospheric modeling, the aerodynamic roughness length, z_0, is considered a control on the latent and sensible heat transfer processes due to its reliance on wind speed, direction, and underlying topographic features [4–6]. Because of this influence, z_0 has a substantial control on snowpack evolution, redistribution, melt rates, and melt water [2,6–8].

      Additionally, snow is the most reflective naturally occurring surface type on Earth and it covers a significant portion of the globe, including as much as 50% of the land mass of the Northern Hemisphere each season. In its pure state snow reflects as much as 98% of incident solar radiation [9,10]. Rough snow absorbs more solar energy than pure snow, which affects both local melt rates as well as the global climate energy budget [11]. As the snow surface roughness increases, it absorbs more solar energy, increasing the snow melt rate and the amount of energy retained in the thermodynamic system. As such, the snowpack surface plays an important role in the Earth's total energy budget through reflection and absorption of solar energy [2,12]. Accurately measuring snow surface roughness is

essential to understanding this interaction with solar radiation and predicting its effects on snowmelt and climate.

Originally defined for studies of wind profiles, z_0 is effectively the height above a surface at which the wind velocity is zero [5,6,13]. Several wind velocities at varying heights are required to quantify z_0 using the wind profile method [5,14]. The measured wind velocities are then plotted against the natural log of the height, resulting in the natural log of z_0 as the y-intercept of the best linear fit. The magnitude of z_0 varies with surface roughness; as surface roughness increases, so does z_0. Fresh snow on a flat, undisturbed surface can have a z_0 as low as 0.0002 meters, reflecting its highly smooth and uniform characteristics. In contrast, the surface of a debris-covered glacier presents a heterogeneous texture, leading to z_0 values that typically range between 0.005 and 0.5 meters [3,15]. These variations indicate the impact of surface properties on aerodynamic roughness, which directly influences snow processes. Given this wide variability, accurately determining z_0 for specific sites is critical to improving the precision of hydrologic and cryospheric models [16,17]. Site-specific values capture variations in land cover, topography, and environmental factors, which generic or averaged estimates cannot adequately represent [17].

Calculating a site-specific z_0 value has historically been challenging due to the reliance on a complex, multi-level wind tower to measure the wind profile [3,14]. These traditional methods, while effective, are labor-intensive, spatially limited, and provide sparse data points. However, advancements in remote sensing technologies have significantly improved the feasibility and accuracy of estimating z_0 over large surface areas [18]. Remote sensing techniques, particularly LiDAR [19] and more recently photogrammetry [44], can integrate the detailed topographic surface and the snowpack surface properties [17,18]. This geometrically based approach enables the calculation of z_0 values across extensive and complex landscapes, providing higher spatial resolution and broader coverage than previously possible. This new methodology of z_0 calculation may supplement or replace traditional techniques of determining z_0.

Aerodynamic roughness length is a calculated parameter which characterizes the loss of wind momentum due to surface roughness [6,21]. For this study, the well-known formula developed by Lettau in 1969 [13] is utilized:

$$z_0 = 0.5 h \frac{s}{S}, \tag{1}$$

where h is the "average vertical extent," or "effective obstacle height," measured in cm, s is the "silhouette area of the average obstacle," measured in cm^2, and S is the "specific area", or "lot area" measured in cm^2 [13]. Figure 1 shows these physical parameters for an idealized case of simple pyramids.
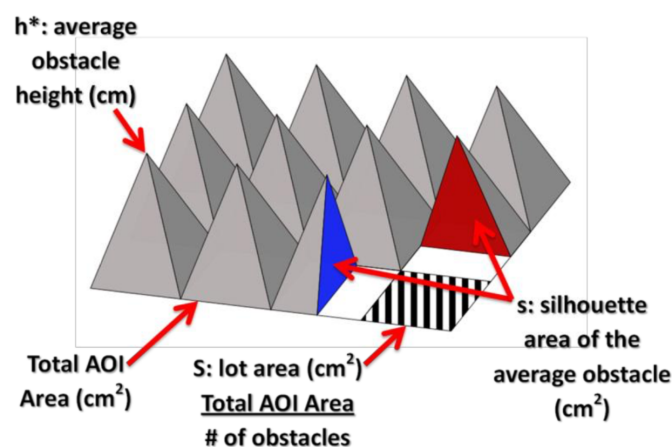

Figure 1. Physical parameters used in Lettau's z_0 formula given by Equation (1). AOI is the Area Of Interest.

This paper presents code to compute z_0 for a surface, provided that the data are on a regular grid. The code can be applied to any surface and at any resolution, and produces the distribution of z_0

values with directionality to consider variable wind directions. Wind direction comes into play in the formula (1) in the determination of the silhouette area *s*. Here, we use three different snow surfaces at different resolutions, as the snow surface, and thus its roughness, can evolve rapidly [8]. We use a fresh snow surface at 1 mm resolution, a snow surface at the time of peak accumulation at 1 m resolution, and a melting snow with sun cups at 5 mm resolution. The three surfaces are initially assessed for an area of 1000 by 1000 pixels and then the resolution is coarsened by an order of magnitude through averaging to a 100 by 100 pixel grid.

2. Methodology

In this section, we describe the method of computing z_0 on LiDAR data. This code takes as input elevation data measured on a regular grid along with a vector indicating the direction the wind is blowing. Since the surface is comprised of obstacles that are nonuniform in shape and size, we approach the z_0 computation element-wise. That is, we consider each obstacle as an individual roughness element.

To compute z_0 we first to segment the surface into roughness elements (the obstacles) $\mathcal{O}_i$, $i = 1 \ldots N$. We then find the lot area S_i, silhouette area s_i, and height h_i of each obstacle. The value of z_0 for the surface as given by Equation (1) is the sum:

$$z_0 = 0.5 \, \Sigma_{i=1}^{N} \frac{h_i}{N} \frac{s_i/N}{S_i/N} = 0.5 \, \frac{1}{N} \Sigma_{i=1}^{N} h_i \frac{s_i}{S_i} \tag{2}$$

We detail our approach below.

2.1. Segmentation into Roughness Elements

One of the challenges when computing z_0 on real-world data is separating individual roughness elements when such elements are of non-uniform shape and size. We approach this problem using the watershed algorithm [22]. The watershed algorithm segments a topographic relief into catchment basins centered around each local minimum. As roughness elements correspond intuitively to local *maxima* of the surface, we first invert the surface. For a surface with points $(x, y, f(x, y))$, the inverted surface consists of the set of points $(x, y, -f(x, y))$. Maxima (minima) of the inverted surface correspond to minima (maxima) of the original surface. Hence, the watershed algorithm applied to the inverted surface yields a segmentation into elements associated to each local maximum of the original surface. These segments are our individual roughness elements, or obstacles.

Intuitively, the watershed algorithm places a marker at each local minimum (maximum in the original data), and floods the relief. The level of the flood is the same increases with time at the same rate in all catchment basins. As the level of the flood increases, eventually the floods originating at two distinct catchment basins will meet, at which point a watershed line is added. The process is continued until the entire relief is flooded and therefore segmented. In our case, each watershed segmentation is associated with a single local maximum, and we consider it to be a single roughness element.

2.2. Computing Areas and Heights

The vertical silhouette area of an obstacle represents the area that is upwind, i.e., the silhouette of the region hit directly by the blowing wind. First, we compute the surface normal vector for every data point using a standard bicubic interpolation in all 3 directions. This takes into account not just immediate neighbors, but nearby data points as well. Projecting each normal vector onto the wind direction vector and retaining only the points that result in a nonzero negative projection indicates data points on the surface that will be hit directly by the wind.

In a single watershed element, we identify all data points which comprise the region hit by the wind and will use them to determine the vertical silhouette area of the obstacle. For each data point determined to be in the upwind region, a general unit square the extent of a pixel is transformed using Rodrigues' formula [23], so that the normal vector of the square is aligned with the normal vector associated with the data point. The square is then projected onto the subspace perpendicular

to the direction of the wind. The area of the resulting parallelogram is computed and contributes to the vertical silhouette. To compute the vertical extent, we again restrict to the data points associated to upwind regions and subtract the minimum height from the maximum height. The lot area is the area of the roughness element, which is easily scaled from the number of points segmented into each watershed.

Using the above quantities, a value for z_0 is computed for each roughness element and averaged over the entire surface. Since there are thousands to tens of thousands of roughness elements per million pixels, the output is also histogram of z_0 values. Further, while the wind direction tends to be consistent, especially over a snow surface [38], the computation can performed directionally.

2.3. Smoothing of the Surface

Two optional modifications may be applied to the data before separating individual roughness features of the surface via the watershed algorithm. An optional Gaussian filter may be applied to the surface (in our code) that smoothens the surface so that there are fewer roughness features associated with small watershed regions. This may help, for instance, in removing small roughness features coming from measurement errors of the surface. This filter smooths by taking a weighted average of neighboring points, where the weight is determined by a symmetric two-dimensional Gaussian (with standard deviation σ) centered at each point. This dampens or removes high frequency features, i.e., small perturbations, and acts as a low-pass filter. This is a common filter choice for smoothing topographical data ([25–28]) and is included as an optional filter in some GIS software ([29,30]). The symmetric 2-D Gaussian smoothing kernel with standard deviation σ is given as

$$G(x,y) - \frac{1}{2\pi\sigma^2}e^{-\frac{x^2+y^2}{2\sigma^2}}, \tag{3}$$

where the size of the filter is given by $2\lceil 2\sigma \rceil + 1$. Additionally, maxima less than a specified percentage higher than the surrounding area may be suppressed resulting in fewer maxima and a simplified watershed profile. This is a common technique in image analysis to reduce over-segmentation ([31]).

3. Datasets and Preparation

3.1. Snow Surface Datasets

The z_0 value was computed for three resolutions of data representing different time periods of the snowpack evolution (accumulation, peak, and ablation) (Table 1 and Figure 2). The fresh snow (FS-FC) dataset was collected during a new snowfall event with snow snowcover existing on the ground. The FS-FC raw point cloud was at a resolution finer than 1 mm. The ablation-sun cup (SC-PH) dataset were collected when substantial sun cups were present during snowmelt. The SC-PH raw point cloud was at a resolution of about 3 mm. Both datasets were collected with a Faro Focus3D X 130 model Terrestrial lidar Scanner (TLS) (https://www.faro.com/). The ablation-sun cup data were collected as three separate scans due to the nature of the surface, i.e., sun cups. The three point cloud were sewn together with Cloud Compare, an open-source software for 3D point cloud and mesh analysis ([32]; https://www.danielgm.net/cc/).

The peak accumulation (PA-NS) data were from the Niwot Saddle behind Boulder, Colorado U.S.A., that is part of the Niwot Long Term Ecological Research Program (https://nwt.lternet.edu/). The point clouds were not available publicly, and the data were already interpolated to a 1-m grid. The data were obtained as per Harpold et al. [33]. All data are available online [34].

The elevation range is larger for the more coarse surfaces (Figure 2d versus Figure 2g and Figure 2a). However, comparing the elevation range (Figures 2c, f and i) to the resolution illustrates less prominence in roughness features as the resolutions becomes larger. Coarsening the resolution of the individual datasets did not alter the elevation distribution, except for the sun cup surface (Figure 2i). These surfaces present three different snowpack conditions with features highlighted by the varying resolutions.
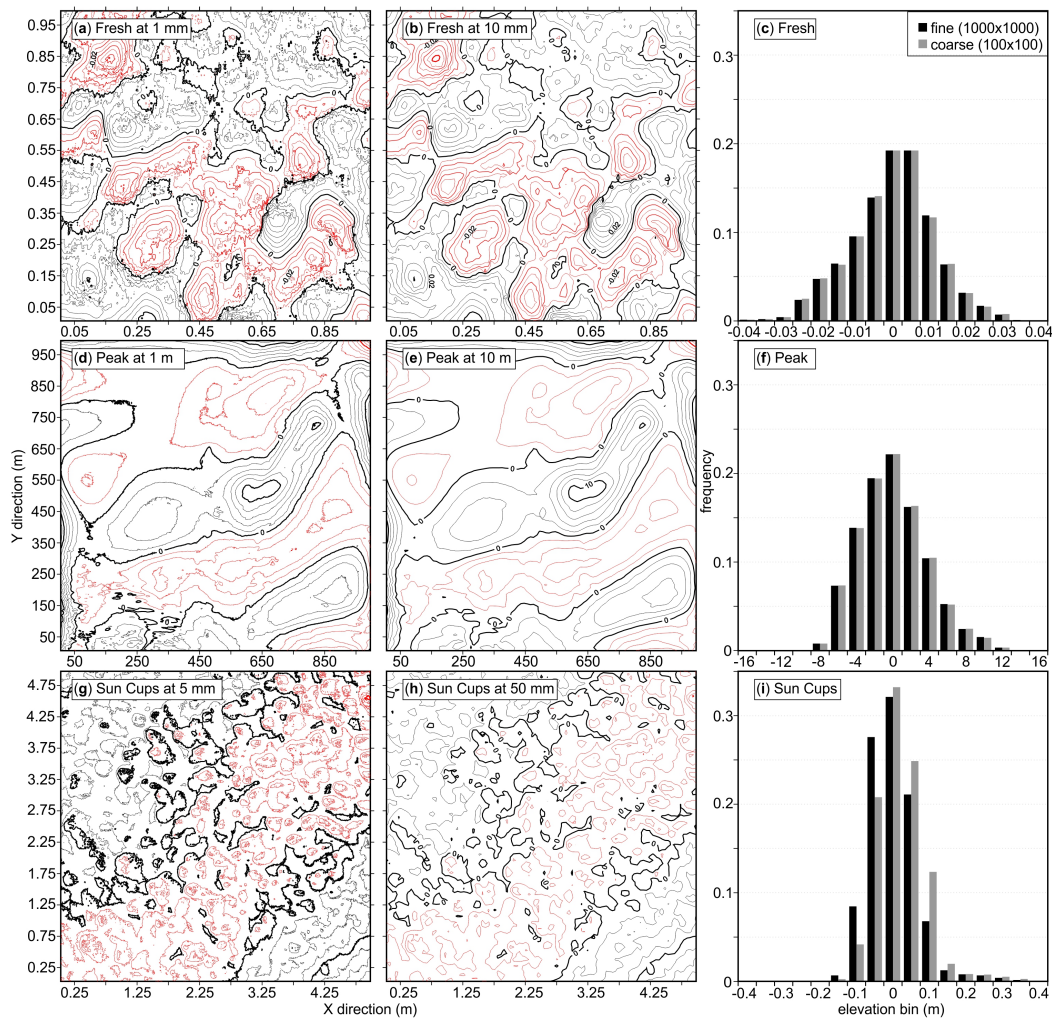
Figure 2. The three gridded datasets used in the z_0 computation as 1000 by 1000 pixels (a, d, g) and coarsened by a factor of 10 (b, e, h), plus the histograms of the distribution of elevation for each surface (c, f, i) for (**a**, **b**, **c**) fresh snow in Fort Collins (lines in 0.005 m intervals), (**d**, **e**, **f**) peak accumulation at Niwot Saddle (lines in 2 m intervals), and (**g**, **h**, **i**) ablation sun cups in the Poudre Headwaters (lines in 0.05 m intervals). The surfaces have been detrended to remove any slope-based bias [35]. As such, black lines/areas are above the datum of zero while red lines/areas are below the datum of zero.

Table 1. Summary of the three datasets used in the z_0 computation. All are for a 1000 by 1000 pixel area at the stated resolution. Data were obtained in the state of Colorado, U.S.A.

dataset	fresh snow	peak accumulation	ablation - sun cups
short name/code	FS-FC	PA-NS	SC-PH
location	Fort Collins	Niwot Saddle	Poudre headwaters
latitude, longitude	40.6, -105.1	40.0547, -105.5890	40.4396, -105.7739
date acquired	19 April 2021	20 May 2010	13 June 2017
resolution (m)	0.001	1	0.05

3.2. Data Preparation

Following the collection of the lidar scans (fresh snow and ablation-sun cup datasets), each raw point cloud (three sewn together for SC-PH) was processed and evaluated using Cloud Compare. The scans were then cropped to the area of interest, ensuring that the dataset was limited to the preferred geographic region or feature under study. Additionally, any rogue points, such as noise or erroneous data points often caused by environmental elements, were identified and removed to enhance the

accuracy and clarity of the dataset. The cropped point cloud was imported into Golden Software's Surfer ([36]; https://www.goldensoftware.com/products/surfer). The software allows the user to interpolate the data using pre-defined methodology, such as kriging, used for this study, and user defined resolutions. The kriging method was chosen because of its capacity to account for the spatial arrangement of measured points, which is relevant to the surface roughness analysis. The result is a smoothed, gridded, surface, instead of the point cloud, which is required to be used within the code.

Each gridded dataset was detrended in the X and Y directions to reduce bias from sloping surfaces [35]. Since the Niwot Saddle covered a hillslope with substantial terrain variation (see [37]), the surface (PA-NS) was detrended three times. First, there was a linear detrend to removed the overall slope. Then, a 3rd-order polynomial was fitted to the surface to remove the saddle feature. Finally, a linear detrend removed the positioning bias.

4. Results

The value of z_0 varied as a function of resolution (Table 2). This is both for the resolution of the original data, i.e., fresh snow versus peak accumulation versus ablation sun cups, and coarsening of the data. There are fewer elements as we coarsen the data, and thus, fewer elements become more granular. For the finest resolution surface (fresh snow), the elements are the smallest.

Most of the roughness elements were small and thus had a low z_0 value (a left skew in Figure 3). For the finer resolution grids (Figures 3a, c, and e), more than 80% of the z_0 value were in the lowest bin. The sun cup surface had the most undulations (Figures 2) c and d), and the most elements at the original and coarsened resolution (Table 2). At smaller scales, there are many more features with a low z_0 value.

The code computes z_0 with directionality, which does vary as a function of coarsening (Figure 4). The smoothest (lowest z_0 values) are not the same direction between the original and coarsened datasets. This is relevant because, while wind tends to blow consistently from the same direction due to terrain influences [38], it does vary [39].

Table 2. Number of elements identified for each datasets and resolution with the mean z_0 value (in cm) for wind blowing from west to east.

surface	fresh snow	-	peak accu-mulation	-	ablation - sun cups	-
resolution (m)	0.001	0.010	1	10	0.005	0.050
elements	7366	195	21090	74	36259	380
mean z_0 (x10^{-3})	0.00054	0.0075	9.4	421	0.012	0.14

As discussed in Section 2.3, two optional parameters, σ and % of maximum height, may be chosen to smoothen the surface before calculating z_0. For the z_0 values reported in Table 2 and Figures 3 and 4, no smoothing was implemented (both smoothing parameters were set to 0). To illustrate how z_0 depends on these parameters, we calculated z_0 for ranges parameter values for the Niwot 1 m data set. Figure 5 shows the results. For small values of σ, z_0 is insensitive to the choice of σ, as seen in the left panel of Figure 5. For larger values of σ, the surface is smoothed to the extent that essential roughness features are lost. Figure 6 illustrates how the watersheds associated with peaks of the surface decrease as σ increases. However, z_0 does depend more sensitively to the % parameter for small values of σ, as seen in the right panel of Figure 5.
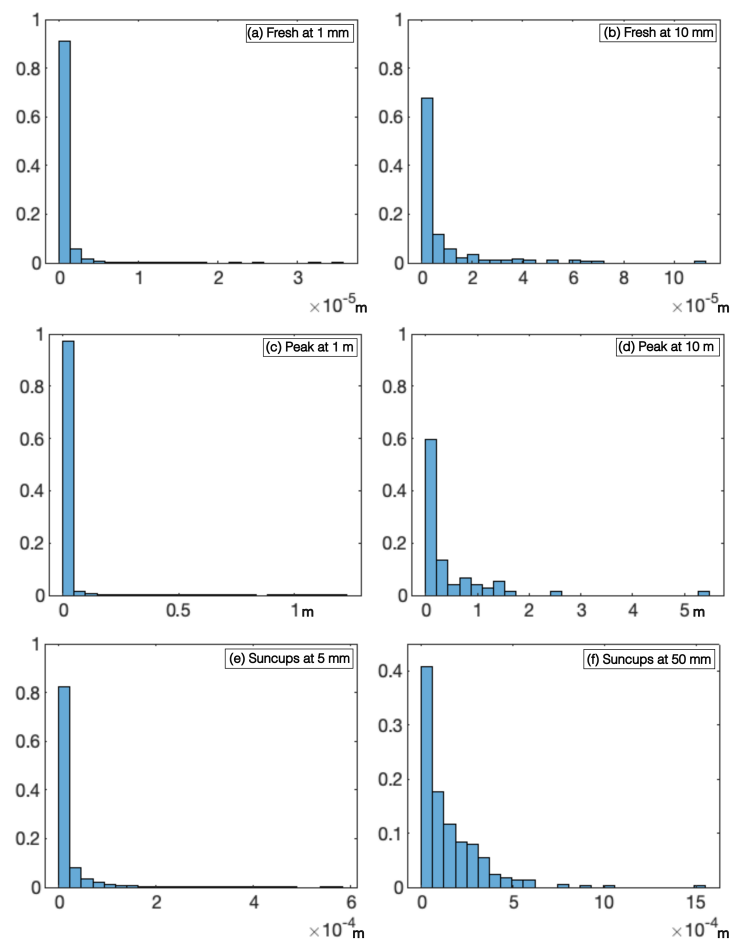
Figure 3. Histogram of z_0 values for the peak accumulation on fresh snow in Fort collins at (**a**) 0.001 m and (**b**) 0.01 m resolutions, the Niwot Saddle (**c**) at 1 m and (**d**) 10 m resolutions, and the ablation sun cups at the Poudre Headwaters at (**e**) 0.005 m and (**f**) 0.05 m resolutions for an eastward wind.
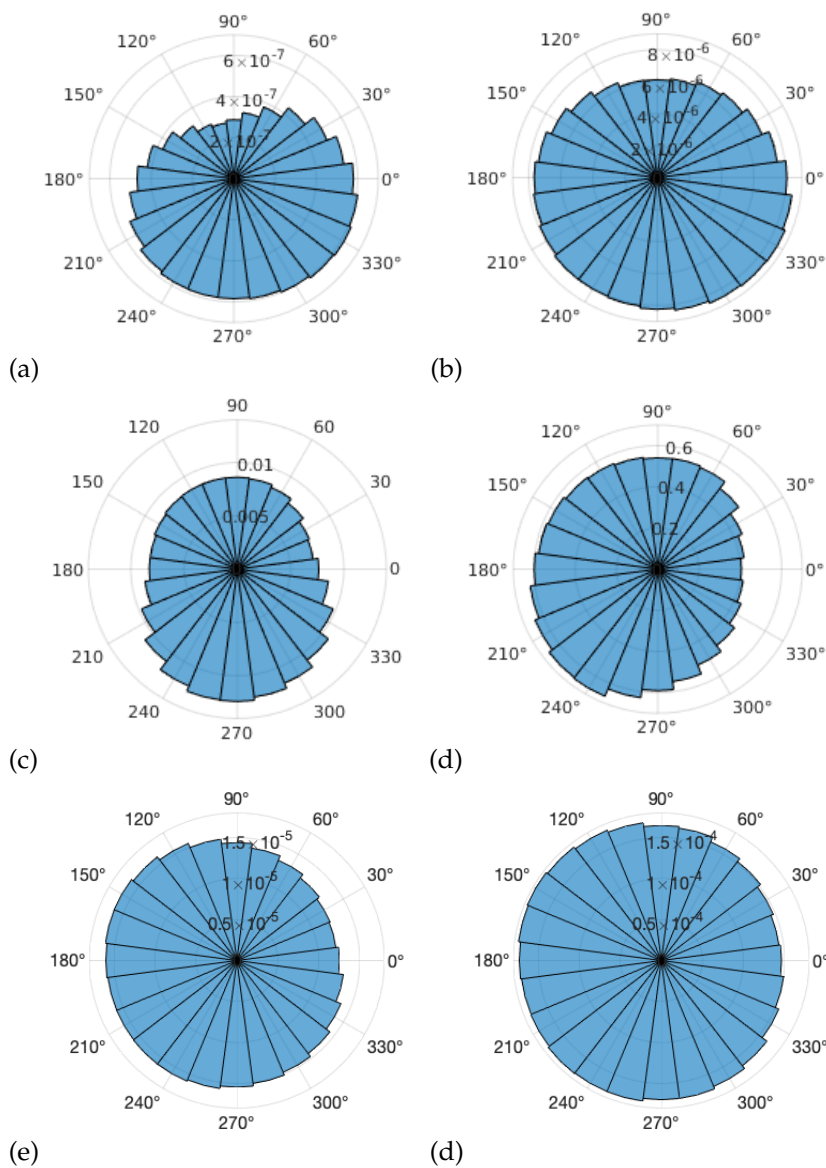
Figure 4. The mean z_0 value varies with the direction from which the wind hits the surface. Shown above is the mean z_0 as it varies with wind direction from 24 different directions for the peak accumulation on fresh snow in Fort Collins at (**a**) 0.001 m and (**b**) 0.01 m resolutions, the Niwot Saddle (**c**) at 1m and (**d**) 10 m resolutions, the ablation sun cups at the Poudre Headwaters at (**e**) 0.005 m and (**f**) 0.05 m resolutions.
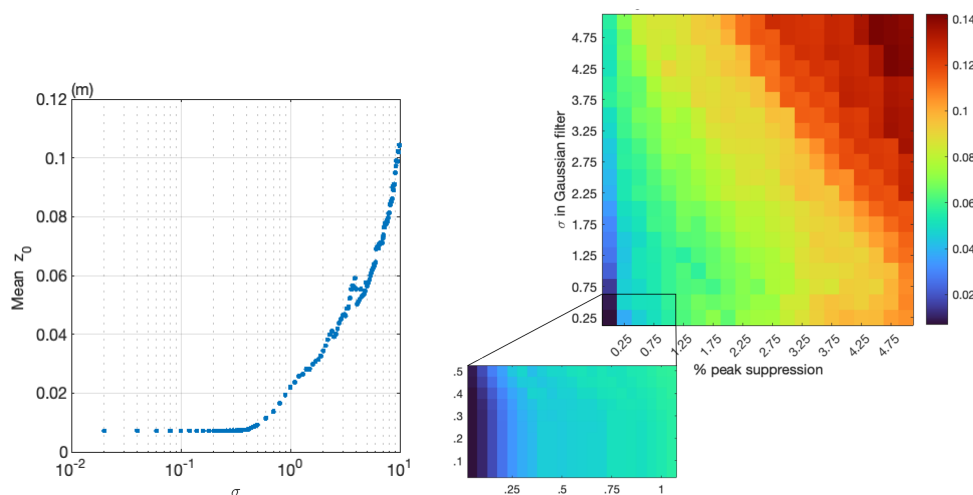
Figure 5. Shown is the sensitivity of the mean z_0 of the Niwot Saddle at 1m resolutions for an eastward wind to changes in the parameter σ (left) in the Gaussian smoothing and to changes in both the % peak suppression parameter and to σ (right) in the preliminary filtering step.
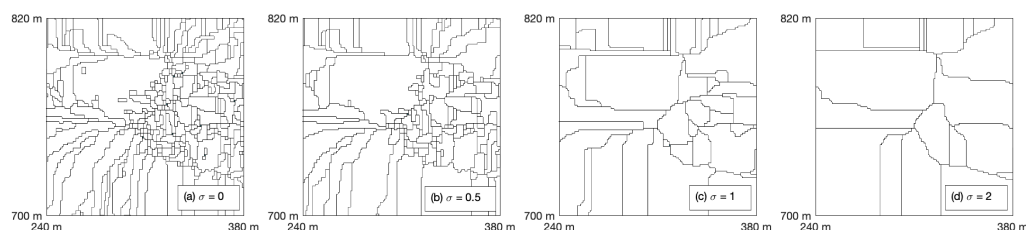
Figure 6. The watershed of a small subset of the Niwot Saddle at 1m resolution for the **(a)** raw data and data filtered via Gaussian smoothing with **(b)** $\sigma = 0.5$, **(c)** $\sigma = 1$, and **(d)** $\sigma = 2$.

5. Discussion

Lettau's formulation [13] of the aerodynamic roughness length z_0, implemented in this paper, is a geometric representation of the surface. There are other formulations [40,41], but they do not appear to be as useful for snow [18]. Lettau's formulation [13] is widely used for snow and glacier surfaces [3,14,42]. With the propensity of spatial surface measurement approaches and data, especially for the snowpack [33,43–45], the geometric estimation of z_0 is a useful approach. As such, this paper provides the computer code to estimate Lettau's [13] z_0 formulation.

Andreas [46] derived an empirical formulation of z_0 for sea ice based on the physical roughness of the surface. It used transect data, based on the dominant wind direction, to compute the roughness. The Andreas [46] approach could be applied to spatial datasets to consider changes in wind direction(Figure 4). Wind directions can vary seasonally and even daily based on weather [39].

Following common approaches in image analysis to reduce effects of measurement noise or oversegmentation, the code includes two optional parameters that smoothen the surface before calculating z_0. The first parameter is the standard deviation σ of the smoothing filter. The second parameter is the % of the maximum height of the surface; peaks with height lower than this percentage height are not included as obstacles contributing to the z_0 calculation. We showed the choice of these parameter values does significantly affect the calculated value of z_0. However, in the case of the Niwot 1 m data set, z_0 is insensitive to the choice σ for small values of σ. The values of these smoothing parameters should be reported in any calculation of z_0 using the Lettau method as implemented in this paper. Further work should elucidate how to choose these parameter values to best match an application, such as using the aerodynamic roughness in a simulation of fluid flow across a surface.

Author Contributions: Conceptualization, R.P., S.R.F., I.O., R.A.N., P.D.S. and J.E.S.; methodology, R.P., R.A.N., P.D.S., S.R.F., and J.E.S.; software, R.P., R.A.N., P.D.S., and J.E.S.; validation, R.A.N., P.D.S., J.E.S. and S.R.F.; formal

Abbreviations

The following abbreviations are used in this manuscript:

AOI is the area of interest

h is the average vertical extent or effective obstacle height, measured in cm

s is the silhouette area of the average obstacle, measured in cm^2

S is the specific area or lot area, measured in cm^2

z_0 is the (geometric) aerodynamic roughness length, measured in m

References

1. Mialon, A.; Fily, M.; Royer, A. Seasonal snow cover extent from microwave remote sensing data: Comparison with existing ground and satellite based measurements. *EARSeL eProceedings* **1994**, *4*, 215-225.

2. Musselman, K.N., Clark, M.P., Liu, C., Ikeda, C., Rasmussen, R. Slower snowmelt in a warmer world. *Nature Climate Change* **2017**, *7*, 214-220 [doi: 10.1038/NCLIMATE3225].

3. Miles, E.S., Steiner, J.F., Brun, F. Highly variable aerodynamic roughness length for a hummocky debris-covered glacier. *Journal of Geophysical Research: Atmospheres* **2017**, *122*,8447-8466 [doi: 10.1002/2017JD026510].

4. Andreas, E. Parameterizing scalar transfer over snow and ice: a review. *Journal of Hydrometeorology* **2002**, *3 (4)*, 417-432 [doi: 10.1175/1525-7541(2002)003<0417:pstosa>2.0.co;2].

5. Gromke, C.; Manes, C.; Walter, B.; Lehning, M.; Guala, M. Aerodynamic roughness length of fresh snow. *Boundary-Layer Meteorology* **2011**, *141 (1)*, 21–34 [doi: 10.1007/s10546-011-9623-3].

6. Smith, M.W. Roughness in the earth sciences. *Earth Science Reviews* **2014**, *136*, 202-225 [doi: 10.1016/j.earscirev.2014.05.016].

7. Andreas, E. L. A theory for the scalar roughness and the scalar transfer coefficients over snow and sea ice. *Boundary-Layer Meteorology* **1987**, *38 (1–2)*, 159–184 [doi: 10.1007/BF00121562].

8. Fassnacht, S. R.; Williams, M. W.; Corrao, M. V. Changes in the surface roughness of snow from millimetre to metre scales. *Ecological Complexity* **2009**, *6 (3)*, 221–229 [doi: 10.1016/j.ecocom.2009.05.003].

9. Kukko, A.; Anttila, K.; Manninen, T.; Kaasalainen, S.; Kaartinen, H. Snow surface roughness from mobile laser scanning data. *Cold Regions Science and Technology* **2013**, *96*, 23 - 35 [doi: 10.1016/j.coldregions.2013.09.001].

10. Zhuravleva, T.B., Kokhanovsky, A. Influence of surface roughness on the reflective properties of snow. *Journal of Quantitative Spectroscopy and Radiative Transfer* **2011**, *112(8)*, 1352-1368 [doi: 10.1016/j.jqsrt.2011.01.004].

11. Amory, C.; Naaim-Bouvet, F.; Gallee, H.; Vignon, E. Brief communication: Two well-marked cases of aerodynamic adjustment of sastrugi. *The Cryosphere* **2016**, *10* [doi: 10.5194/tc-10-743-2016].

12. Thackeray, C.W., Fletcher, C.G. Snow albedo feedback: Current knowledge, importance, outstanding issues and future directions. *Progress in Physical Geography: Earth and Environment* **2016**, *40 (3)*, [doi: https://doi.org/10.1177/0309133315620999].

13. Lettau, H. Note on aerodynamic roughness-parameter estimation on the basis of roughness-element description. *Journal of Applied Meteorology* **1969**, *8*, 828-832 [doi: 10.1175/1520-0450(1969)008<0828:NOARPE>2.0.CO;2].

14. Munro, D. S. Surface roughness and bulk heat transfer on a glacier: comparison with eddy correlation. *Journal of Glaciology* **1989**, *35(121)*, 343–348 [doi:10.3189/s0022143000009266].

15. Brock, B.; Willis, I.; Sharp, M. Measurement and parameterization of aerodynamic roughness length variations at Haut Glacier d'Arolla, Switzerland. *Journal of Glaciology* **2006**, *52 (177)*, 281–297 [doi: 10.3189/172756506781828746].

16. Fassnacht, S. R. Temporal changes in small scale snowpack surface roughness length for sublimation estimates in hydrological modelling. *Cuadernos De Investigación Geográfica* **2010**, *36 (1)*, 43 [doi: 10.18172/cig.1226].

17. Sanow, J.E.; Fassnacht, S.R.; Suzuki, K. How does a dynamic surface roughness affect snowpack modelling? *Polar Science* **2024**, *41(1-2)*, [doi: 10.1016/j.polar.2024.101110].

18. Sanow, J.E., Fassnacht, S.R., Kamin, D.J., Sexstone, G.A., Bauerle, W.L., Oprea, I. Geometric versus anemometric surface roughness for a shallow accumulating snowpack. *Geosciences* **2018**, *8(12)*, 463 [doi: 10.3390/geosciences8120463].

19. Hood, J.L.; Hayashi, M. Assessing the application of a laser rangefinder for determining snow depth in inaccessible alpine terrain. Hydrology and Earth System Sciences 2010, 14(6), pp.901-910.

44. Nolan, M.; Larsen, C.; Sturm, M. Mapping snow depth from manned aircraft on landscape scales at centimeter resolution using structure-from-motion photogrammetry. The Cryosphere 2015, 9(4), pp.1445-1463.

21. Jacobson, M.Z. Fundamentals of atmospheric modeling. 2nd ed.; Cambridge University Press: Cambridge, Great Britain, 2005; 978-0-521-54865-6.

22. Meyer, F. Topographic distance and watershed lines. *Signal processing* **1994**, *38 (1)*, 113-125.

23. Encyclopedia of Mathematics: Rodrigues formula. Available online: https://encyclopediaofmath.org/wiki/Rodrigues formula (accessed on 30 December, 2024).

38. Winstral, A.; Elder, K.; Davis, R. E. Spatial snow modeling of wind-redistributed snow using terrain-based parameters. Journal of Hydrometeorology 2002, 3(5), 524-538.

25. Lindsay, J.B. Whitebox GAT: A case study in geomorphometric analysis. Computers & Geosciences, **2016** 95, 75-84. [doi: 10.1016/j.cageo.2016.07.003]

26. Lindsay, J. B., Francioni, A., Cockburn, J. M. H. LiDAR DEM Smoothing and the Preservation of Drainage Features. *Remote Sensing* **2016**, *11(16)*, 1926. [doi:10.3390/rs11161926]

27. O'Neil, G. L., Saby, L., Band, L. E., & Goodall, J. L. Effects of LiDAR DEM smoothing and conditioning techniques on a topography-based wetland identification model. Water Resources Research, **2019**, 55(5), 4343-4363.

28. Erdbrügger, J., van Meerveld, I., Bishop, K.,Seibert, J. Effect of DEM-smoothing and-aggregation on topographically-based flow directions and catchment boundaries. Journal of Hydrology, **2021**, 602, 126717.

29. Whitebox Tools. Available online: https://www.whiteboxgeo.com/.

30. Conrad, O., Bechtel, B., Bock, M., Dietrich, H., Fischer, E., Gerlitz, L., Wehberg, J., Wichmann, V., and Böhner, J.: System for Automated Geoscientific Analyses (SAGA) v. 2.1.4, Geosci. Model Dev., **2015** 8, 1991-2007, doi:10.5194/gmd-8-1991-2015.

31. The MathWorks, Inc. Imhin Documentation. mathworks.com. Accessed: October 5, **2024**. Available online: https://www.mathworks.com/help/images/ref/imhmin.html

32. CloudCompare. Available online: https://www.danielgm.net/cc/ (accessed on 30 December, 2024).

33. Harpold, A. A.; et al. LiDAR-derived snowpack data sets from mixed conifer forests across the Western United States. Water Resour. Res. 2024, 50, 2749–2755, doi:10.1002/2013WR013935.

34. Fassnacht, S.R.; Sanow, J.E. Fresh Snow and Ablation-Sun Cup Snow Surface Datasets for Evaluation of Geometry Aerodynamic Roughness Code [Dataset]. Dryad 2025. https://doi.org/10.5061/dryad.qv9s4mwr2

35. Fassnacht, S. R.; Stednick, J. D.; Deems, J. S.; Corrao, M. V. Metrics for assessing snow surface roughness from digital imagery. Water Resources Research 2009, 45, W00D31. https://doi.org/10.1029/2008WR006986

36. Golden Software – Surfer. Available online: https://www.goldensoftware.com/products/surfer/ (accessed on 30 December, 2024).

37. Sexstone, G. A.; Fassnacht, S. R.; López-Moreno, J. I.; Hiemstra, C. A. Subgrid snow depth coefficient of variation spanning alpine to sub-alpine mountainous terrain. Cuadernos de Investigación Geográfica/Geographical Research Letters 2022, 48(1), 79-96. https://doi.org/10.18172/cig.4951

38. Winstral, A; Marks D. Simulating wind fields and snow redistribution using terrain-based parameters to model snow accumulation and melt over a semi-arid mountain catchment. Hydrological Processes 2002, 16(18), 3585-603. https://doi.org/10.1002/hyp.1238

39. Moron, V.; Robertson, A.W.; Qian, J.-H.; Ghil, M. (2015). Weather types across the Maritime Continent: from the diurnal cycle to interannual variations. Front. Environ. Sci. 2015, 2, 65. [doi: 10.3389/fenvs.2014.00065]

40. Counihan, J. Wind tunnel determination of the roughness length as a function of the fetch and the roughness density of three-dimensional roughness elements. Atmos. Environ. 1971, 5, 637–642. https://doi.org/10.1016/0004-6981(71)90120-X

41. Macdonald, R.W.; Griffiths, R.F.; Hall, D.J. An improved method for the estimation of surface roughness of obstacle arrays. Atmos. Environ. 1998, 32, 1857–1864. https://doi.org/10.1016/S1352-2310(97)00403-2

42. Nield, J.M.; King, J.; Wiggs, G.F.; Leyland, J.; Bryant, R.G.; Chiverrell, R.C.; Darby, S.E.; Eckardt, F.D.; Thomas, D.S.; Vircavs, L.H.; Washington, R. Estimating aerodynamic roughness over complex surface terrain. Journal of Geophysical Research: Atmospheres 2013, 118(23), pp.12-948. https://doi.org/10.1002/2013JD020632

43. Revuelto, J.; López-Moreno, J.I.; Azorín-Molina, C.; Zabalza, J.; Arguedas, G.; Vicente-Serrano, S.M. Mapping the annual evolution of snow depth in a small catchment in the Pyrenees using the long-range terrestrial laser scanning. Journal of Maps 2014, 10(3), pp.379-393. https://doi.org/10.1080/17445647.2013.869268

44. Nolan, M.; Larsen, C.; Sturm, M. Mapping snow depth from manned aircraft on landscape scales at centimeter resolution using structure-from-motion photogrammetry. The Cryosphere 2015, 9, 1445–1463. https://doi.org/10.5194/tc-9-1445-2015

45. Revuelto, J.; Alonso-Gonzalez, E.; Vidaller-Gayan, I.; Lacroix, E.; Izagirre, E.; Rodríguez-López, G.; López-Moreno, J.I. Intercomparison of UAV platforms for mapping snow depth distribution in complex alpine terrain. Cold Regions Science and Technology 2021, 190, p.103344. https://doi.org/10.1016/j.coldregions.2021.103344

46. Andreas, E.L. A relationship between the aerodynamic and physical roughness of winter sea ice. Q. J. R. Meteorol. Soc. 2011, 137, 1581–1588. https://doi.org/10.1002/qj.842

47. z_0 Lettau LiDAR Watershed Code. [GitHub Repository] Available online: https://github.com/rneville/Z0-Lettau-LiDAR-Watershed **2025**.